J. COMBIN. MATH. COMBIN. COMPUT. 127a (2025) 7829--7859

Journal of Combinatorial Mathematics and Combinatorial Computing
www.combinatorialpress.com/jcmcc

Combinatorial Press

Research on reliability analysis and optimization strategy of turning process in aerospace manufacturing based on fuzzy mathematics

Wenbo Shi[1], Haiyang Liu[2,3,4,✉], Jie Liu[3], Changyou Li[5]

[1] International Engineering College, Shenyang Aerospace University, Shenyang, Liaoning, 110136, China
[2] College of Aerospace Engineering, Shenyang Aerospace University, Shenyang 110136, China
[3] Department of Research Engineering, AVIC SAC Commercial Aircraft Co., Ltd, Shenyang, 110000, China
[4] Key Laboratory of Fundamental Science for National Defense of Aeronautical Digital Manufacturing Process of Shenyang Aerospace University, Shenyang, Liaoning, 110136, China
[5] School of Mechanical Engineering and Automation, Northeastern University, Shenyang 110819, China

ABSTRACT
In this paper, the Gamma process is used to describe the change of cutting force coefficient and analyze the time-varying stability of chattering, and then the time-varying reliability model of chattering of turning machining system is established. The optimal Coupla function model is selected by the AIC criterion, and the reliability analysis of the turning machining system is carried out by using the Monte Carlo method and the VC-MCS method which introduce the Coupla function, and at the same time, the fuzzy factors of the turning machining process are taken into consideration, and the fuzzy optimization mathematical model of turning machining is set up with the goal of the lowest machining cost, and then the model is solved by using the multi-objective particle swarm optimization algorithm, which realizes the fuzzy optimization in the aerospace manufacturing. Then the model is solved using a multi-objective particle swarm optimization algorithm to realize the reliability optimization of turning machining process in aerospace manufacturing, and the fuzzy optimization mathematical model of turning machining is experimentally verified by taking common plane milling and cylindrical turning as an example. The experimental results show that the analysis results of the VC-MCS method and the Monte Carlo method with the introduction of Coupla function are almost the same, which verifies that ignoring the correlation between the parameters affects the turning reliability results, and secondly, the turning machining system operates well at full rotational speeds when the turning width b=0.63mm. Finally, according to the case results, the effectiveness and feasibility of the proposed optimization method is proved, which can provide certain optimization objectives for improving the efficiency of turning machining.

✉ Corresponding author.
E-mail address: shiwenbo2025@126.com (H. Liu).
Received 15 January 2024; Revised 20 February 2024; Accepted 30 November 2024; Published Online 15 April 2025.
DOI: 10.61091/jcmcc127a-432

Keywords: turning machining, Coupla function, Monte Carlo method, fuzzy optimization, particle swarm optimization

1. Introduction

The aviation industry requires a high degree of precision and reliability of components, and everything must be safe and reliable. The reliability of aircraft components is directly related to the safety of flight, and each component is interrelated, the quality and performance of a component will directly affect the performance of the entire system [1-2]. Therefore, the machining process of components must be safe and reliable, and turning can meet these requirements. In the manufacture of aircraft engines, fuselages, rudder surfaces and other components, turning machining is widely used in titanium alloys, aluminum alloys, high-temperature alloys, stainless steel and other metal materials [3-5].

Turning machining is an important machining process, which is widely used in automotive, general machinery, and other fields in addition to aerospace [6-7]. It can realize precision machining of various shapes and sizes, such as external, internal, flat and curved surfaces, with an accuracy of 0.005 mm [8]. And the integrity of the cutting surface significantly affects the fatigue life, creep strength, wear resistance and other properties of the parts [9]. Through reasonable tool selection and parameter adjustment, it can meet the machining needs of different workpieces and ensure the quality of parts processing. Different processes and tool selection can flexibly meet the machining needs of a variety of different shapes and sizes of workpieces. Turning processing can be carried out at the same time multi-tool, parallel cutting, greatly improving the processing efficiency, and in the optimization of the processing path through the tool to reduce the loss of cutting time and cutting force, further improving the processing efficiency [10-11]. In addition, facing different materials, such as steel, copper, aluminum, magnesium and other metal materials, as well as plastics, wood, ceramics and other non-metallic materials, turning machining has good adaptability. Its process is relatively mature, simple to operate and easy to control the accuracy [12]. It is a very reliable machining method for mass-produced parts machining. At the same time, turning machining can further improve the stability and reliability of machining through the application of automated equipment and CNC systems [13-14]. However, during turning machining, due to the use of high-speed rotating tools, deformed materials, tool wear, and uncertainties involving high temperatures and high pressures, various safety hazards lurk, which have an impact on the reliability of the machining process [15-16]. Fuzzy mathematics is a new branch of mathematics that uses mathematical methods to study and deal with the phenomenon of vagueness, which provides a new way to deal with the problem of uncertainty and imprecision, and it is a powerful tool for describing the human brain's thinking to deal with fuzzy information [17]. Fuzzy mathematics is used to characterize the uncertainty parameters in the turning machining process, to analyze and evaluate the reliability of the machining dynamics, and to propose machining optimization strategies to support the quality and efficiency of the turning machining process in aerospace manufacturing.

In the study, the reliability of turning process in aerospace manufacturing is firstly simulated using Monte Carlo method based on Copula function, and Kendall rank correlation coefficient is used to visualize the correlation between the metric variables. Based on the Kendall rank correlation coefficient, the relevant parameters of the Copula function are calculated, and the optimal Copula function is selected using the AIC criterion. Then the fuzzy optimization mathematical model of turning dosage with the goal of lowest processing cost is established in consideration of the fuzzy factors affecting the turning process, and the multi-objective particle swarm algorithm is used to solve the problem to realize the optimization of the reliability of the turning process, and finally the feasibility and validity of the model is proved by combining with the example calculations.

2. Reliability analysis of turning process in aerospace manufacturing

2.1. Reliability analysis methods

2.1.1. Monte Carlo simulation. Monte Carlo simulation method, also known as probabilistic simulation method and random sampling method. The method is based on two laws of large numbers, and reliability analysis is achieved through statistical experiments or stochastic simulations. It is one of the most accurate and applicable probabilistic methods for mechanical systems [18]. The method consists of a sampling design space based on mean and variance, and a probability density function for random variables. Reliability is defined as the ratio of the number of samples in the safe region to the total number of samples. Compared with other methods, the Monte Carlo simulation method has the advantages of high generality and high computational accuracy.

Let the engineering structure function be:

$$Z = g(x) = g\left(x_1, x_2, \cdots, x_n\right) \tag{1}$$

Thus the structural limit state equation $g\left(x_1, x_2, \ldots, x_n\right) = 0$ can divide the variable space into two parts, the reliability region and the failure region, and the failure probability P_f is:

$$P_f = \int \cdots \int_{g(x) \le 0} f_X\left(x_1, x_2, \cdots, x_n\right) dx_1 dx_2 \cdots dx_n \tag{2}$$

where $f_X\left(x_1, x_2, \ldots, x_n\right)$ is the joint probability density function (PDF) of the underlying random variable $x = \left(x_1, x_2, \ldots, x_n\right)^T$.

If the parameters of each random variable are independent of each other, the failure probability P_f is equivalently converted to:

$$P_f = \int \cdots \int_{g(x) \le 0} f_{X_1}\left(x_1\right) f_{X_2}\left(x_2\right) \cdots f_{X_n}\left(x_n\right) dx_1 dx_2 \cdots dx_n \tag{3}$$

where $f_{Xi}\left(x_i\right)(i = 1, 2, \ldots, n)$ is the probability density function of the fundamental parameter x_i.

In general, the limit state function in engineering practice is usually difficult to write the expression, and some of them are multi-dimensional complex integrals, which are difficult to get the analytical solution. And Monte Carlo simulation method can avoid this problem.

The basic idea of this method for solving the failure probability P_f is to generate N random samples $x_\tau(\tau = 1, 2, \ldots, N)$ from the joint probability density function $f_X(x)$ of the input variables x, substitute these random samples into the structure function function $g(x)$, and count the number of samples that fall into the failure region, denoted as N_f. The failure probability N_f / N in the random samples can be equated to the failure probability P_f as a whole. ie:

$$\begin{aligned} P_f &= \int \cdots \int_R I_f(x) f_X\left(x_1, x_2, \cdots, x_n\right) dx_1 dx_2 \cdots dx_n \\ &= E\left(I_f(x)\right) \approx \frac{N_f}{N} \end{aligned} \tag{4}$$

where $I_f(x) = \begin{cases} 1, & x \in \Box \\ 0, & x \notin \Box \end{cases}$.

Denotes the indicator function; $\Box$ denotes the multidimensional variable space; and $E(\cdot)$ denotes the mathematical expectation.

The Monte Carlo simulation method requires multiple executions of deterministic simulations, and it is simple and easy to implement. However, due to its slow convergence speed, it needs to consume a lot of simulation time to ensure its high computational accuracy, therefore, Monte Carlo simulation method is mainly used to verify the probabilistic analysis results of other algorithms.

2.1.2. Weibull and Copula Functions. The Weibull distribution provides a comprehensive description of the stages of the bathtub failure rate curve and is one of the most widely used models for life reliability analysis of mechanical equipment. When the parameters in the Weibull distribution are different, it can be metamorphosed into exponential, normal and Rayleigh distributions. The probability density function $f(t)$ and its distribution function $F(t)$ of the two-parameter Weibull distribution are:

$$f(t)=\frac{m}{\eta}\left(\frac{t}{\eta}\right)^{m-1}\mathrm{e}^{-\left(\frac{t}{\eta}\right)^{m}} \tag{5}$$

$$F(t)=1-\mathrm{e}^{-\left(\frac{t}{\eta}\right)^{m}} \tag{6}$$

where, t is the lifetime random variable; η is the scale parameter, also known as the characteristic lifetime parameter in engineering, which gives the approximate location of the points in the distribution curve; and m is the shape parameter, which determines the shape of the distribution curve.

The Copula function is also known as the connection function. From the n-dimensional Sklar's theorem, if F is the joint distribution function of random variables $X_1, X_2, \cdots, X_n$ and the marginal distribution function of each random variable is $F_1, F_2, \cdots, F_n$, then there must exist an n-dimensional Copula function C with $F(x_1, x_2, \cdots, x_n)=C(F_1(x_1)$, $F_2(x_2), \cdots, F_n(x_n))$ for any $x \in R^n$; if $F_1, F_2, \cdots, F_n$ is continuous, then function C is unique. This theorem shows that the joint distribution function of any multidimensional random variable can be divided into two parts: the one-dimensional marginal distribution of each random variable and the Copula function.

The Archimedean family of Copula functions is widely used to describe the joint distribution of multidimensional random variables. The Gumbel Copula function, Clayton Copula function and Frank Copula function are also widely used. Since the Frank Copula function is not suitable for describing the correlation between random variables with asymmetric structure, the Gumbel Copula function and Clayton Copula function are widely used to deal with the case where the marginal distribution is a Weibull distribution. Therefore, the Gumbel Copula and Clayton Copula functions are chosen for fitting and the optimal fitting function model is selected with the expressions:

$$C^{Cum}=e^{-\left(\sum_{n=1}^{N}(-\ln u_n)^{\frac{1}{\theta}}\right)\theta}, 0<\theta\leq 1 \tag{7}$$

$$C^{Cla}=\left(\sum_{n=1}^{N}u_n^{-\delta}-N+1\right)^{-\frac{1}{\delta}}, 0<\delta<+\infty \tag{8}$$

where u_n obeys a uniform distribution on $[0,1]$ if $u_n(n=1,2,\cdots,N)$ is a continuous unitary marginal distribution function.

2.1.3. Parameter estimation. The great likelihood estimator for a lifetime time sample of $t_1, t_2, \cdots, t_N$ obtained from the probability density function of the Weibull distribution is:

$$\begin{aligned}\ln L(t_1, t_2, \cdots, t_N; m, \eta) &= -m\cdot N\cdot \ln\eta + N\cdot\ln m \\ &+(m-1)\cdot\sum_{n=1}^{N}\ln t_n-\frac{1}{\eta^m}\cdot\sum_{n=1}^{N}t_n^m\end{aligned} \tag{9}$$

The two great likelihood estimates $\hat{m}$ and $\hat{\eta}$ of the Weibull distribution can be obtained by using Eq. (9) to obtain the partial derivatives of m and η, respectively.

From the probability density function $c(u_1,u_2,\cdots,u_n;\theta)$ and the marginal density function $f_n(t_n;\varepsilon_n)(n=1,2,\cdots,N)$ of the Copula function, the probability density function of the joint distribution function is calculated as:

$$f(t_1,t_2,\cdots,t_N;\theta)=c(u_1,u_2,\cdots,u_N;\theta)\prod_{n=1}^{N} f_n(t_n;\varepsilon_n) \tag{10}$$

where $c(u_1,u_2,\cdots,u_N;\theta)=\dfrac{\partial C(u_1,u_2,\cdots,u_N)}{\partial u_1,u_2,\cdots,u_N}$, θ are the parameters of the Copula function and $u_n=F_n(t_n;\varepsilon_n)$, $\varepsilon_n(n=1,2,\cdots,N)$ are the parameters of the N marginal distribution function.

The great likelihood estimation function for a life time sample of $t_{1m},t_{2m},\cdots,t_{Nm}(m=1,2,\cdots,M)$ obtained from this probability density function is:

$$\begin{aligned}\ln L(t_1,t_2,\cdots,t_N;\theta)=\sum_{m=1}^{N}\Bigg[&\sum_{n=1}^{N}\ln f_n(t_{nm};\varepsilon_n)\\&+\ln c\big(F_1(t_{1m};\varepsilon_1),F_2(t_{2m};\varepsilon_2),\cdots,F_N(t_{Nm};\varepsilon_N);\theta\big)\Bigg]\end{aligned} \tag{11}$$

The great likelihood estimate of the Copula function $\hat{\theta}$ is obtained by taking the partial derivative of θ according to equation (11).

2.1.4.Bare Pool Informativeness Guidelines. Akaike informativeness criterion (AIC) is a measure of the goodness of fit of statistical models to the data, built on the basis of "entropy", applicable to the estimation of parameters by the great likelihood estimation method, the smaller the value of the better the fit [19]. The specific expression is as follows:

$$AIC=-2\ln A+2m \tag{12}$$

where A is the value of the great likelihood function in the model and m is the number of independent parameters in the model.

2.2. Modeling of turning dynamics in aerospace manufacturing

2.2.1. Turning dynamics modeling. Figure 1 shows a sketch of the single-degree-of-freedom (SDoF) regenerative chatter dynamics model of the turning machining system. Since the tool system is the main vibration system of the turning machining system, and the dynamic change of cutting width is only caused by the regenerative chatter, the dynamic differential equation of the turning machining system is

$$m\ddot{q}(t)+c\dot{q}(t)+kq(t)=\Delta F(t)\cos(\varphi-\alpha) \tag{13}$$

where: m, c and k are the equivalent mass kg, equivalent damping $(N\cdot s/m)$ and equivalent stiffness (N/m) of the turning system, respectively; $\Delta F(t)$ is the dynamic cutting force; φ is the angle between the cutting force and the tool vibration direction; α is the angle between the main vibration direction and the tool vibration direction.

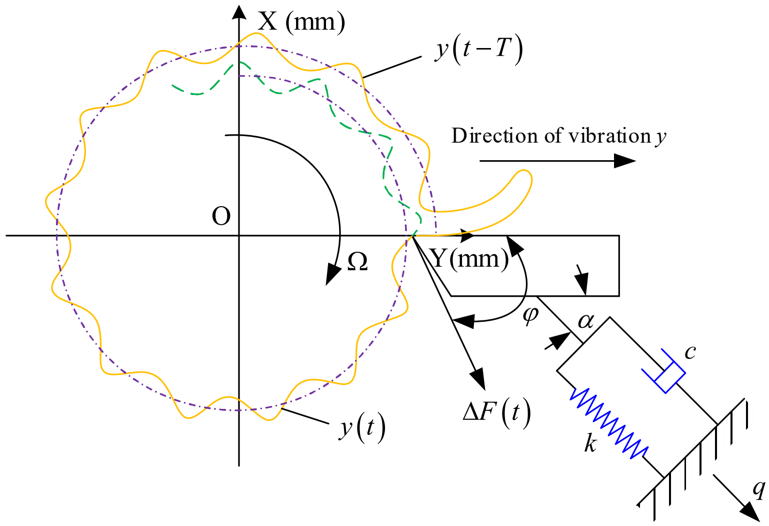

Fig. 1. The mechanical model of the turning of the car

The dynamic cutting force ensemble is determined by the dynamic change of cutting width, so the expression for the dynamic cutting force ensemble is:

$$\Delta F(t) = K_s(t) \cdot a_p \cdot h(t) = K_s(t) \cdot a_p \cdot [\eta y(t-T) - y(t)] \tag{14}$$

where: a_p for the cutting width (mm); $h(t)$ for the cutting thickness variation (mm); η for the turning machining overlap coefficient, $0 < \eta < 1$; $y(t)$ for the current moment of turning vibration displacement (mm); $y(t-T)$ for the last turn when the turning vibration displacement (mm); T for the spindle rotation period (s), $T = 60/\Omega$, Ω for the spindle speed $(r/\min)$.

From Fig. 1, it can be seen that the relationship between the vibration displacement in the direction of tool vibration and the vibration displacement in the direction of the main vibration is $y(t) = u(t) \cdot \cos\alpha$, and assuming that the vibration displacement of turning machining is expressed as $y(t) = A\sin(\omega t + \varphi_0)$, and the initial conditions are all 0, the differential equations of the dynamics of turning machining, which take into account the wear of the tool, will be subjected to Laplace transformation:

$$\begin{aligned} s^2 y(s) + \left[2\omega_n \xi - \frac{K\eta \sin(\omega T)}{\omega}\right] s y(s) \\ + \left[\omega_n^2 - K(1 - \eta\cos(\omega T))\right] y(s) = 0 \end{aligned} \tag{15}$$

where: $s = \sigma + i\omega$ is the root of the characteristic equation; $K = -\omega_n^2 K_s a_p u / k$; ω_n is the intrinsic frequency of the turning machining system, $\omega_n^2 = k/m$; ξ is the damping ratio of the turning machining system, $\xi = c/2m\omega_n$; u is the directional coefficient, $u = \cos(\varphi - \alpha)\cos\alpha$.

2.2.2. Turning chatter time-varying stability. According to the Nyquist stability criterion, the system is in the critical state of stability and instability when the real part of the root of the characteristic equation shown in Eq. (15) is $\sigma = 0$, i.e., $s = i\omega$, and the time-varying limiting cutting width in the critical state is solved as:

$$a_{p\lim} = \frac{k\left[\left(1-\lambda^2\right)^2 + (2\xi\lambda)^2\right]}{K_n(t)u\left(\lambda^2-1\right)} \cdot \frac{1-\eta\cos\left[2j\pi + \arcsin\dfrac{2\xi\lambda}{\eta\sqrt{(2\xi\lambda)^2+\left(1-\lambda^2\right)^2}} - \arctan\left(\dfrac{2\xi\lambda}{1-\lambda^2}\right)\right]}{1+\eta^2-2\eta\cos\left[2j\pi + \arcsin\dfrac{2\xi\lambda}{\eta\sqrt{(2\xi\lambda)^2+\left(1-\lambda^2\right)^2}} - \arctan\left(\dfrac{2\xi\lambda}{1-\lambda^2}\right)\right]} \tag{16}$$

The corresponding spindle speed is:

$$\Omega = \frac{60\lambda\omega_n}{2j\pi + \arcsin\dfrac{2\xi\lambda}{\eta\sqrt{(2\xi\lambda)^2+\left(1-\lambda^2\right)^2}} - \arctan\left(\dfrac{2\xi\lambda}{1-\lambda^2}\right)} \tag{17}$$

where: $\lambda = \omega/\omega_n$, due to the system vibration frequency ω is slightly greater than the intrinsic frequency of the system ω_n, $\lambda > 1$; $j = 0,1,2,\cdots$, is the number of leaf valves.

2.3. Time-varying reliability analysis of turning chatter in aerospace manufacturing

2.3.1.Time-varying reliability model of turning chatter. In the actual turning process, due to measurement errors and environmental factors, turning chatter stability analysis needs to take into account the randomness of the parameters, turning chatter reliability is the probability of the turning processing system does not chatter, that is, the probability that the turning processing limit cut width is greater than the given cut width.

The turning chatter time-varying reliability limit state function is:

$$g(S(t),t) = a_{p\lim}(t) - a_p \tag{18}$$

where: a_p is the given cutting width; $S(t) = [X, Y(t)]$ is the sample point of the turning machining system parameter, X is the random variable about the turning machining system parameter x, $x = \left[k,c,m,\varphi,\alpha,\eta\right]^T$, $Y(t) = \left(K_s(t),\Omega(t)\right)$ are the cutting force coefficients and spindle speed random process.

Turning machining system from 0 to t moments in the occurrence of chatter can be expressed as:

$$E = \left\{\exists\,\tau \in [0,t] \middle| g\left(S(t),\tau\right) \le 0\right\} \tag{19}$$

Therefore the cumulative failure probability of the system from 0 to t moment is $P_F\left(0,t\right) = \Pr ob\left(E\right)$. The time-varying reliability model of turning chatter is:

$$R\left(0,t\right) = 1 - P_F\left(0,t\right) = 1 - \Pr ob\left(E\right) \tag{20}$$

2.3.2. Monte Carlo Reliability Analysis Method with Copula Functions. When a system is a series system, the reliability of the system can be analyzed by applying a Monte Carlo method that introduces a Copula function. The key of the method is to model random variables with Copula function structure. As an example, the four-dimensional Copula function is introduced to analyze the reliability of a system consisting of four units. Take T_1, T_2, T_3, T_4 as the four lifetime random variables of the joint distribution function, and their marginal distribution functions are the reliability functions of the four units, i.e., $U=R_1(t_1)$, $V=R_2(t_2)$, $W=R_3(t_3)$, $X=R_4(t_4)$. Since the random variables U, V, W, X obey the uniform distribution on $[0,1]$, the random variables can be constructed by starting from U, V, W, X, and the main steps are as follows:

1) Find the Copula functions $C(U,V)$, $C(U,V,W)$, and $C(U,V,W,X)$ separately.

2) Simulate four mutually independent pseudo-random numbers u, b, c, and d on the interval $[0,1]$.

3) When $U=u$, V of the conditional distribution function $C(V\mid u)=\frac{\partial C(U,V)}{\partial U}|U=u$, from which the inverse function of the conditional distribution function to $v=C_u^{-1}(b)$. When $U=u$, $V=v$, W of the conditional distribution function $C(W\mid u,v)=\frac{\partial C(U,V,W)}{\partial U\partial V}|U=u,V=v$, from which the inverse function of the conditional distribution function to $w=C_{u,v}^{-1}(c)$. When $U=u$, $V=v$, $W=w$, X of the conditional distribution function $C(X\mid u,v,w)=\frac{\partial C(U,V,W,X)}{\partial U\partial V\partial W}|U=u,V=v,W=w$, from which the inverse function of the conditional distribution function to $x=C_{u,v,w}^{-1}(d)$.

4) The inverse function of the marginal distribution yields $t_1=R_1^{-1}(u)$, $t_2=R_2^{-1}(v)$, $t_3=R_3^{-1}(w)$, $t_4=R_4^{-1}(x)$, where t_1, t_2, t_3, t_4 are the lifetime random variables with Copula function structure.

2.4. *Analysis of examples*

2.4.1. Sample analysis and modeling of optimal distributions. Next, VC-MCS method is adopted to analyze the reliability of the turning machining system. From the reliability model established earlier, it is known that the main parameters considered in the analysis process include m, c, k, etc. The specific test data are shown in Table 1. The data is obtained by using the desktop lathe CJ0625 as the test platform, through the test as well as the component analysis method.

Table 1. Test sample values and system mode parameters

$f_n(HZ)$	$m(kg)$	$c(N.s/m)$	$k(N/m)$	$r(rpm)$
133.5	13.29	1538.12	8710000	2996.5
134	12.45	1429.87	7930000	3005.8
134.5	11.84	1385.91	7710000	3002.8
134.5	12.53	1411.62	8070000	2998.8
134	12.19	1498.58	8290000	3001.7
134	12.65	1434.97	8150000	2999.7
134.5	12.54	1411.59	8090000	3002.9
134.5	11.58	1347.11	7550000	3002.8
134.5	11.58	1347.11	7550000	3002.8
134.5	11.86	1368.55	7650000	3000.7
135	12.25	1411.32	7960000	2997.7
133.5	13.53	1545.87	8740000	3000.7
133.5	13.28	1553.87	8570000	3002.8
133.5	13.91	1585.54	8950000	3000.5
133.5	13.19	1493.31	8480000	3002.5
134	13.14	1493.31	8510000	3001.5
134	12.84	1467.72	8310000	2998.6
133	13.55	1576.11	8650000	3001.5

133	14.27	1571.87	8410000	3002.5
134	13.31	1503.67	8570000	2998.3

First, analyze the sample, through the sample analysis, to find the variables with correlation, at the same time, determine the positive and negative correlation as a preliminary screening Copula function criteria. The sample distribution is shown in Figure 2. As can be seen from the figure, it can be inferred that there is a clear positive correlation between the cutting parameters m, c and k, and these judgments can be used as a preliminary selection of suitable criteria for Copula, which is only a preliminary judgment, in order to be more accurate, the Kendall rank correlation coefficient is used to quantitatively measure the correlation between each parameter, and it can be used as a basis for the calculation of correlation parameters for the Copula function later. The results of the Kendall rank correlation coefficient are shown in Table 2. Combined with the nature of the Kendall rank correlation coefficient, it can be concluded from the table that there is a strong or weak correlation between parameters m, c, and k.

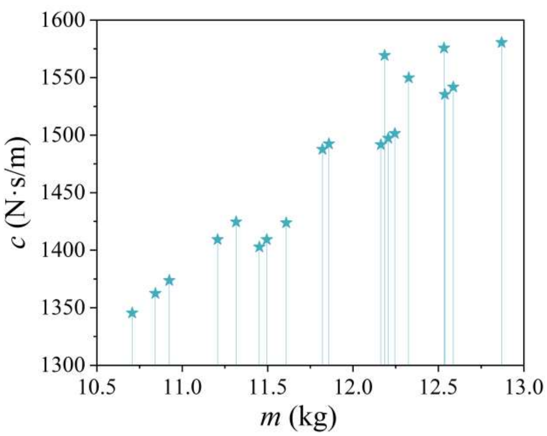

(a) Distribution 1

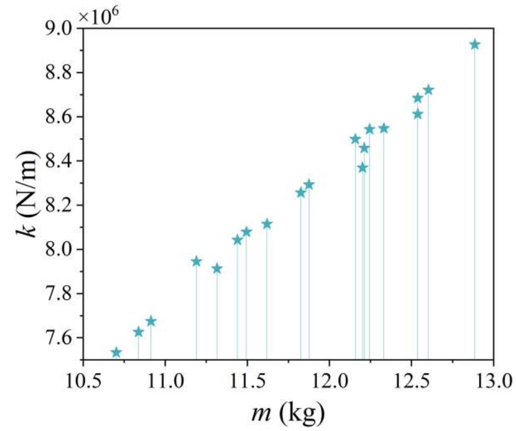

(b) Distribution 2

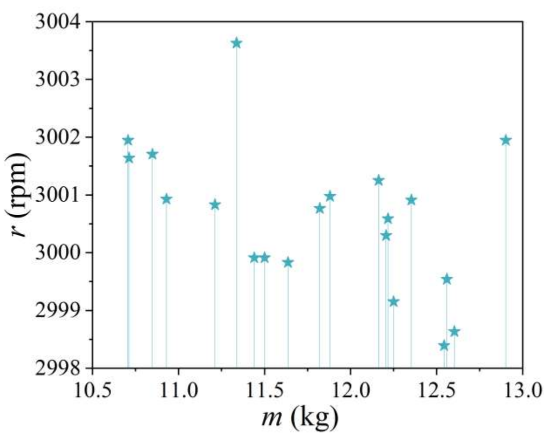

(c) Distribution 3

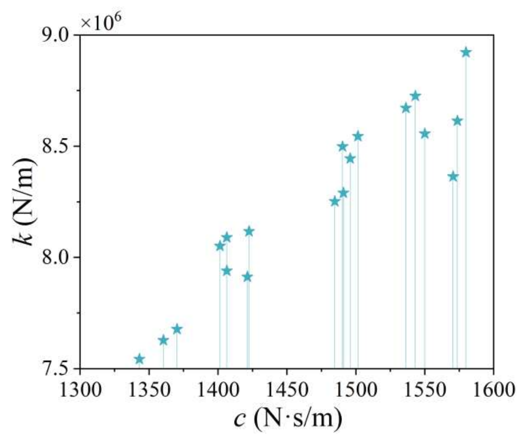

(d) Distribution 4

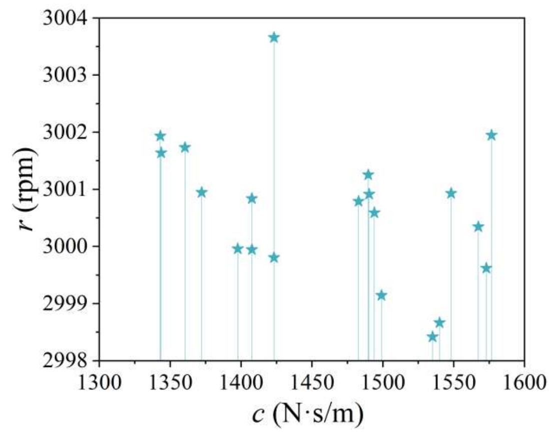

(e) Distribution 5

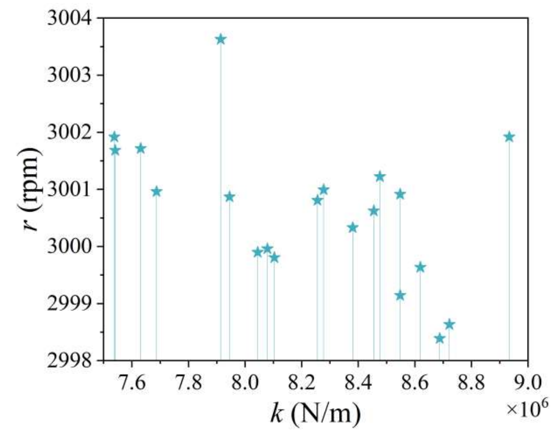

(f) Distribution 6

Fig. 2. Sample distribution of random variables

Table 2. Two and two kendall rank correlation coefficients for random variables

Variable	m and c	m and k	c and a
The Kendall rank correlation coefficient	0.8677	0.9768	0.8352

Next, it is necessary to find out the relevant parameters of each alternative Copula function and select the optimal Copula function to describe the correlation between the variables m, c, and k. The AIC criterion and the BIC criterion are used to select the optimal distribution, and the Copula function with the smallest values of AIC and BIC is the optimal one for fitting the correlation structure of the original observed data, and the AIC and BIC values between the two of each variable are shown in Table 3. The AIC and BIC values between each variable are shown in Table 3. Based on the AIC and BIC values between each parameter in the table, the respective optimal Copula structure can be determined, and the selection results are shown in Table 4. Meanwhile, the same AIC criterion is used to judge the optimal marginal distribution function of each variable, and the AIC values of each variable are shown in Table 5, and the calculation results are shown in Table 6. The process also needs to use the joint probability density function between different conditional probability distributions, and the correlation between each conditional distribution function is still relevant, therefore, it is necessary to choose the appropriate Copula structure to describe the correlation characteristics between the conditional probability distributions, and the same use of the AIC criterion for selection, and the AIC values of the different Copula functions are shown in Table 7. The optimal Copula function selection results between each conditional distribution are shown in Table 8.

Table 3. AIC and BIC values for different copula functions and between different variables

	Gaussian Copula	No.16 Copula	Clayton Copula	Gumbel Copula	Frank Copula
The AIC value between m and c	-39.1458	Inf	-56.6831	-32.0975	-42.5173
The BIC value between m and c	-38.2871	Inf	-55.7549	-31.1109	-41.5538
The AIC value between m and k	-69.3421	Inf	-70.6492	-78.0528	-65.7614
The BIC value between m and k	-68.4387	Inf	-69.6149	-77.0825	-64.3352
The AIC value between c and k	-36.7159	Inf	-50.4371	-28.9835	-36.1148
The BIC value between c and k	-35.7177	Inf	-49.4578	-27.9175	-35.0964

Table 4. Optimal copula function among individual variables

Variable	m and c	m and k	c and k
Optimal copula function	Clayton Copula	Gumbel Copula	Clayton Copula

Table 5. AIC values of different distributions of individual variables

	Normal distribution	Log-normal distribution	Extreme value I type distribution	Weibull distribution
M variable AIC	45.2788	45.5739	49.0257	955.3981
The c variable V	235.8248	235.8763	238.1948	1147.62
K variable AIC	578.6359	578.8941	583.3081	1499

Table 6. Probability distribution properties of the random variables

Fundamental variable	Mean	Standard deviation	Distribution pattern
Variable m	12.4752	0.6859	Normal distribution
Variable c	1531	80.4841	Normal distribution
Variable k	8.2798×10^{6}	4.6729×10^{5}	Normal distribution

Table 7. AIC values between the individual conditional probability distributions

AIC	Gaussian Copula	No.16 Copula	Clayton Copula	Gumbel Copula	Frank Copula
C13/2(fm/c and fk/c)	2.6178	12.7329	-	-	0.8645

Table 8. Optimal copula function between the individual conditional probability distributions

Variable	C13/2(fm/c and fk/c)
Copula function	Frank Copula

2.4.2. Turning system machining process stability analysis. The dynamic parameters of the turning system obtained from the sample analysis; m, c, k, ω_n, K_S are substituted into the formula to find out the limiting cutting width corresponding to different spindle speeds, and then the leaf flap diagrams of the stability of the turning chatter simulated under the conditions of these parameters are plotted as shown in Fig. 3. The lower part of the curve in the figure is the stable region, when the turning system is in the stable region represents that it can run stably and is reliable, as long as it is located in this region, no matter how high the spindle speed is, the turning system is reliable. Below the curve is the chatter region, i.e. the failure region, when located in the chatter region represents that the system will fail. The point on the blade curve represents the critical state, also known as the conditionally stable region, which means that the system itself is able to operate stably under these conditions, but when the conditions change, such as when subjected to some kind of incentive, it will be easy to fail.

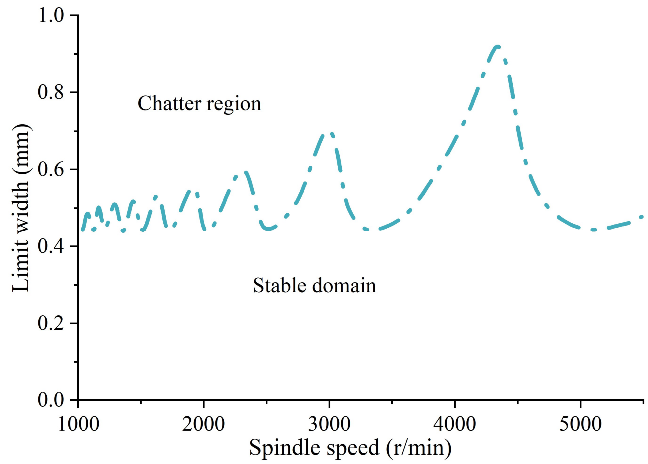

Fig. 3. Turning stability lobe diagram

2.4.3. Turning system machining process reliability analysis. The optimal Copula function between the selected parameters and the optimal marginal distribution of each parameter are brought into the formula to establish the joint probability density function of the machine tool turning vibration system, and the reliability analysis of the turning system is carried out on the basis of the multi-dimensional correlation variable reliability calculation method established earlier, combined with the vibration stability leaf flap diagram.

Firstly, the VC-MSS method is used for calculation, and the specific flow chart is shown in Figure 4.

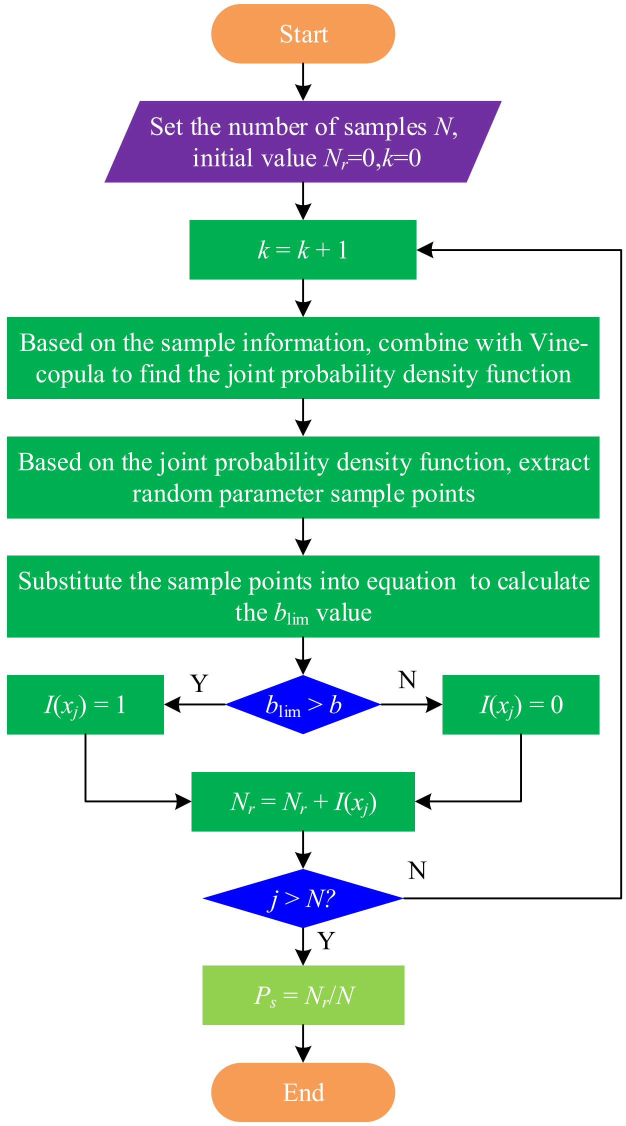

Fig. 4. Flowchart of the vc-mss method of chatter reliability

The reliability lobe loft of the stability of the turning chatter system is plotted as shown in Fig. 5, which is plotted in three cases where the actual cutting width is b=0.67mm, b=0.65mm, and b=0.63mm, respectively. As can be seen from the figure, with the increase of the given turning width, the chattering stability gradually becomes worse, when the turning width is the largest, b = 0.67mm, the turning chattering stability is poor, relatively the most prone to chattering, the minimum value of the degree of reliability is only 0.4308, and it is only stable in the main leaf flap area; when the turning width is reduced to b = 0.65mm, the possibility of chattering of the system is reduced, and it is clearly When the turning width is reduced to b=0.65mm, the possibility of chattering of the system is reduced, and it is obviously stabilized, and the minimum value of reliability reaches 0.7841. When the turning width is b=0.63mm, the stability of turning chatter is the best, and the instability is the smallest, and the minimum value of reliability is 0.9698, and the turning machining system operates well under the full rotational speed.

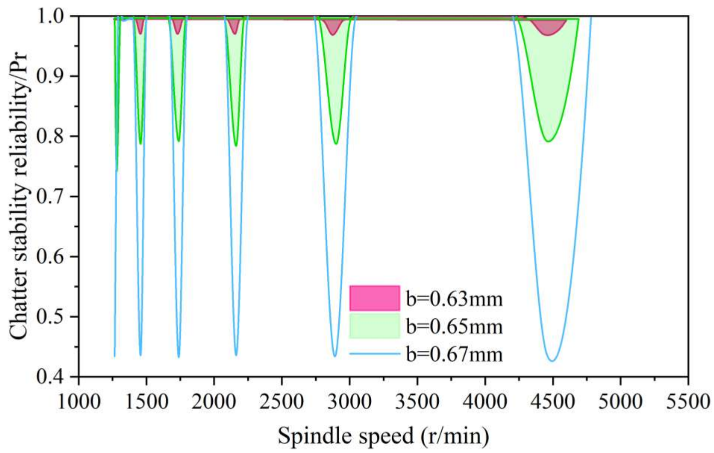

Fig. 5. Reliability of lathe shear and vibration stability by VC-MSS method

Next, the reliability of the chattering system is analyzed using the Monte Carlo method proposed in this paper using the introduction of the Copula function, and the reliability curves are plotted as shown in Fig. 6. Then the reliability values solved by the two methods are compared specifically, and the minimum value of reliability under different cutting widths is compared, and the results are shown in Table 9, which shows that the reliability values calculated by using the VC-MSS method are basically the same as those by the proposed method, but the efficiency of the Monte Carlo method with the introduction of the Copula function is much improved, which also shows the practicability of the method.

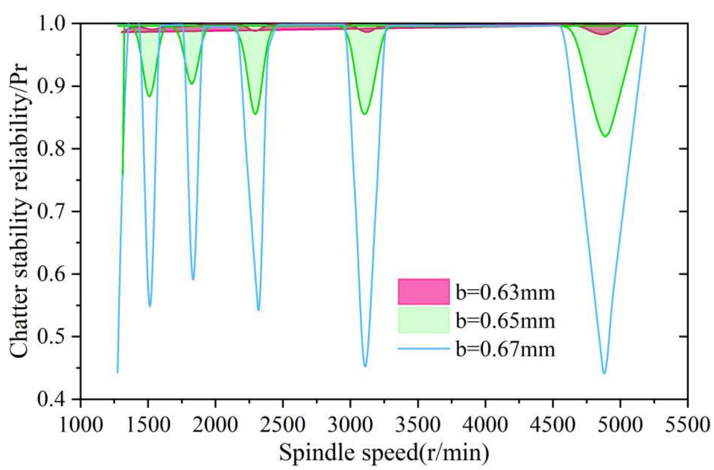

Fig. 6. Monte Carlo method for lathe cutting vibration stability reliability

Table 9. Comparison of minimum reliability between the two methods

Cutting width b(mm)	Reliability	
	VC-MCS method	Monte Carlo method
b=0.63mm	0.9711	0.9725
b=0.65mm	0.7834	0.7847
b=0.67mm	0.4318	0.4351

Under the same given cut width condition, the reliability curves of turning chatter stability in two cases of considering the correlation between parameters and not considering the correlation are shown in Fig. 7, from which it can be clearly seen that the correlation has a very obvious influence on the reliability of chatter stability, for example, when considering the correlation, the minimum value of the reliability is 0.4312, and the minimum value of the reliability of the turning system without considering the correlation is enlarged to 0.4806; This also shows the necessity of studying the correlation between the parameters of the turning machining system.

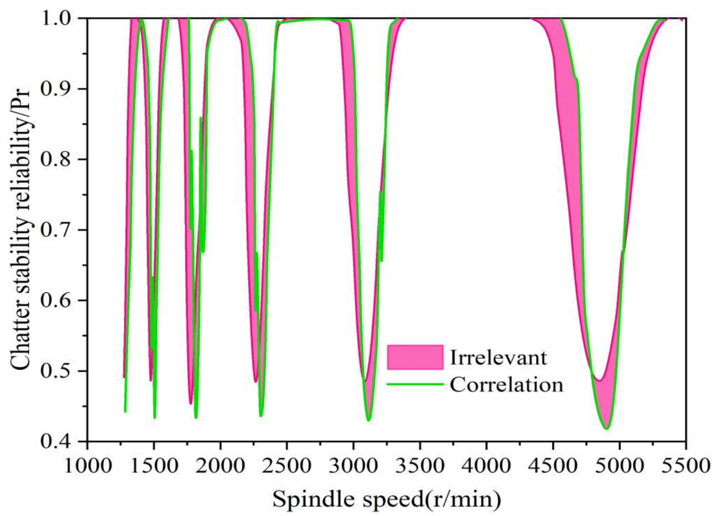

Fig. 7. Reliability of lathe shear chatter stability under related and unrelated conditions

2.4.4. Comparison of simulated and sample points. In order to verify the fitting ability of the Gumbel Copula function model to the original sample and the accuracy of the simulation points, the simulation points of each parameter of the turning system were compared with the original observation data, and the specific comparison results are shown in Table 10 and Table 11, it can be seen that the simulation points obtained by sampling have almost the same degree of correlation with the original sample points, and the probability density characteristics of each variable simulated are almost the same as those of the original sample data. Thus, the correctness of the sample simulation is illustrated.

Table 10. Comparison of kendall rank correlation coefficients between simulated points and sample point

Variable	m and c	m and k	c and k
Raw observation data τ	0.8674	0.9657	0.8327
Simulated sample point τ	0.8667	0.9761	0.8331

Table 11. Comparison of the probability distribution properties of the random variables

Fundamental variable	Raw observation data		Simulated sample point	
Variable m	Mean	Standard deviation	Mean	Standard deviation
Variable c	11.7865	0.6791	11.7813	0.6799
Variable k	1472	79.5945	1468	79.0591
Fundamental variable	8.2207×10^{6}	4.2157	8.2175×10^{6}	4.1661×10^{5}

In order to see more intuitively the correctness of the sample simulation, Fig. 8 shows the scatter plots of the simulated points (blue pentagrams) of the different variables against the sample points when the number of simulations N = 500, from which it can be seen that the simulated points of the individual variables fit the sample points very well, both in terms of their shapes and their change trends.

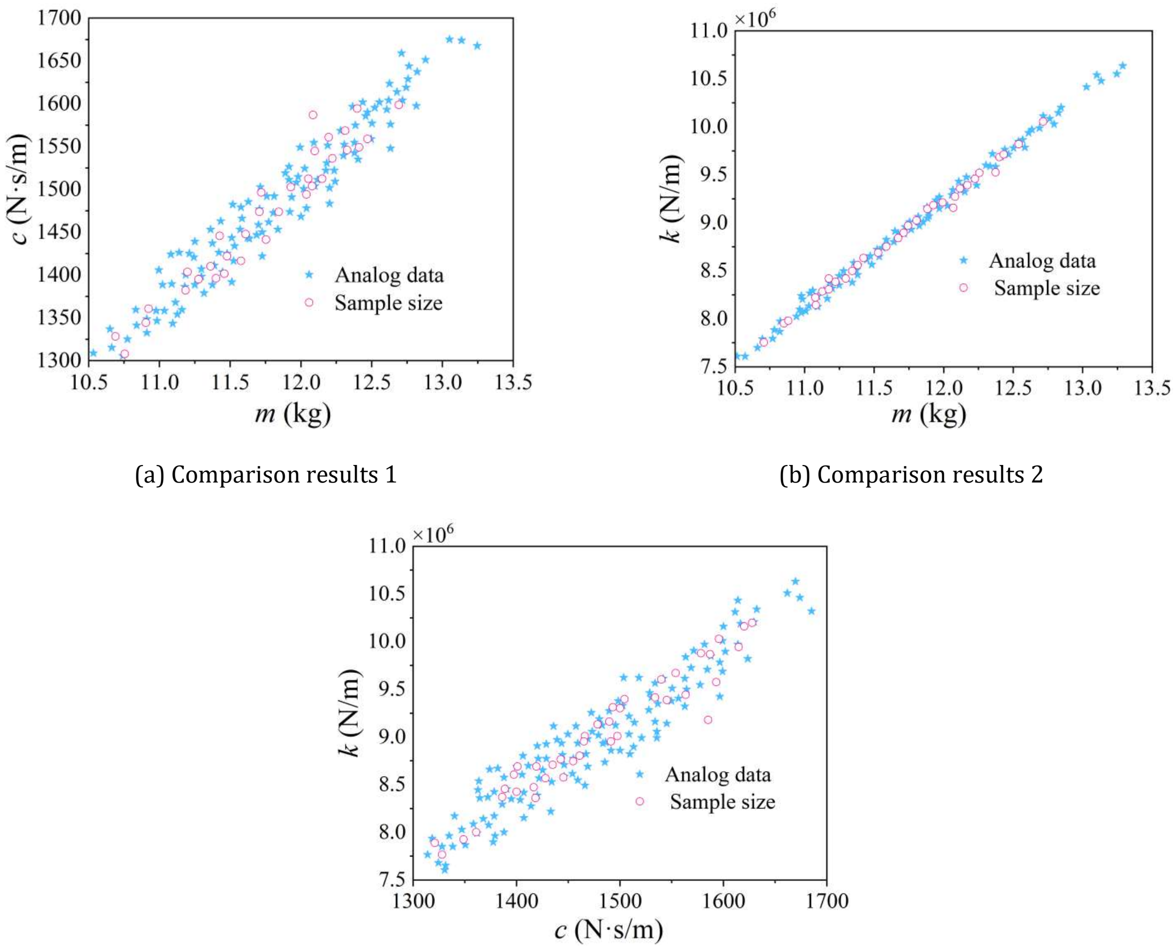

(a) Comparison results 1

(b) Comparison results 2

(c) Comparison results 3

Fig. 8. Simog points and sample points between different variables

3. Reliability optimization of turning machining process based on fuzzy mathematics

3.1. Fuzzy mathematics and reliability optimization methods

3.1.1. Basic concepts of fuzzy mathematics. Probability theory and mathematical statistics extend the application of mathematics from the realm of necessary phenomena to the realm of random phenomena, while fuzzy mathematics expands the explicit phenomena to the realm of fuzzy phenomena [20]. Since its inception, fuzzy mathematics has basically formed a relatively complete system.

L.A. zadeh obtained the definition of a fuzzy set by generalizing the characteristic function of an ordinary set from set $\{0,1\}$ to the closed interval $[0,1]$.

Let the domain be U, A be its ordinary subset, and for some element u, $u \in A$, or $u \notin A$ in U either one or the other. This defines the mapping μ_A from U to $\{0,1\}$:

$$U \to \{0,1\}, u \to A(u) = \begin{cases} 1 & u \in A \\ 0 & u \notin A \end{cases} \tag{21}$$

where $A(u)$ is the characteristic function of the ordinary subset A, also denoted as $C_A(u)$

Let the mapping μ_A from U to $\{0,1\}$ be defined on the domain U:

$$\mu_A : U \rightarrow \{0,1\}, u \mapsto \tilde{A}(u) \in [0,1] \tag{22}$$

Then $\tilde{A}$ is said to be a fuzzy (Fuzzy) set on U, and $\tilde{A}(u)$ is said to be the affiliation function of $\tilde{A}$, also denoted as $\mu_{\tilde{A}}(u)$, which is called the degree of affiliation of u with respect to $\tilde{A}$, and indicates the degree to which u belongs to $\tilde{A}$.

When $\mu_{\tilde{A}}(u)$ takes only 0 and 1, the fuzzy set $\tilde{A}$ degenerates to $\tilde{A}$, and $\tilde{A}(u)$ is the characteristic function of A. It can be seen that ordinary sets are only special cases of fuzzy sets, and fuzzy sets can contain ordinary sets, and from the definition of fuzzy sets, we know that fuzzy set $\tilde{A}$ is uniquely determined by its affiliation function $\mu_{\tilde{A}}(u)$, and therefore, fuzzy sets and their affiliation functions can be viewed as equivalent. The idea of the affiliation function (degree of affiliation) reflects the intermediate excess state in fuzziness and is carried out throughout fuzzy mathematics.

3.1.2. Reliability optimization methods. The so-called Reliability-Based Design Optimization (RBDO) is a design methodology based on reliability analysis and combined with an optimal design model. The feasibility of its design refers to the reliability constraints or the probability of constraint satisfaction.

In general, the reliability optimization design mathematical model can be expressed as:

$$\begin{cases} \min f(X) \\ s.t. P\{g_i(X) \geq 0\} \geq R_i, (i=1,2,\cdots,m) \\ q_j(X) \leq 0, (j=1,2,\cdots,l) \\ h_k(X) = 0, (k=1,2,\cdots,n) \end{cases} \tag{23}$$

In Eq. (23), $f(X)$ is the objective function, X is the basic random variable, R_i represents the target reliability to be satisfied (given the reliability threshold), and $q_j(X)$ and $h_k(X)$ are the inequality and equation constraint matrices, respectively.

The traditional approach to solving reliability optimization problems is usually to implement a two-layer optimal design strategy: the outer layer performs the uncertainty analysis, the inner layer performs the reliability assessment, and multiple iterations are performed until the probabilistic objectives and constraints are satisfied. Therefore, this two-layer strategy brings the disadvantages of high computational effort and low efficiency. A novel single-layer loop method, the Serial Optimization and Reliability Assessment (SORA) method, avoids nested loops for optimization as well as reliability assessment.

The SORA method implements a serial single-loop strategy that is able to decouple the outer structural optimization from the inner reliability analysis. In the execution of the current loop, the MPP points obtained from the previous loop are substituted for the random variables (in the execution of the first loop step, the mean value of the random variables is used as the initial optimization point), and the new design points are obtained through the structural deterministic optimization problem. After the deterministic optimization has been solved, reliability analysis is performed to verify that all the inverse MPP points meet the reliability requirements. If not, the obtained inverse MPP points are applied to further improve the constraints by shifting the boundaries of the constraint functions to ensure that the optimization is performed in the feasible domain.

3.2. Establishment of fuzzy optimization mathematical model

3.2.1. Determination of design variables. In the turning process, when the workpiece material to be machined, machining machine and machining tools have been fixed, need to determine the amount of turning machining is turning speed v, plus depth a_p, feed f. So determine the design variables for:

$$X=\left[x_1,x_2,x_3\right]^T=\left[v,a_p,f\right]^T \tag{24}$$

3.2.2. Determination of the objective function. In normal production conditions, time is relatively generous, the objective function of optimizing the amount of turning machining is usually selected for each workpiece process processing costs. Therefore, the objective function is determined as:

$$F_{(t)}=C=t_m\cdot M+t_{ct}\frac{t_m}{T}\cdot M+\frac{t_m}{T}\cdot C_t+t_{ut}\cdot M \tag{25}$$

where t_m - Cutting and machining time of the process (maneuvering time)/min.

t_{ct} - Time required for one tool change/min.

t_u - Other auxiliary time other than tool change / min.

M - The number of factory-wide costs per unit of time apportioned to the process /yuan.

C_t - Costs associated with the tool during tool endurance (including the cost of adding the tool to the plant) /$/unit.

T - Tool endurance/min.

3.2.3. Establishment of fuzzy constraints. In the turning process, turning machining amount of choice is not arbitrary, they are subject to machine power, machining surface roughness, tool durability, machine tool spindle speed and feed mechanism and other production conditions of the various constraints. These constraints can be categorized into two main aspects: performance constraints and geometric constraints. In this paper, these constraints are regarded as fuzzy subsets of the design space, and the fuzzy constraints are established as follows:

1) The constraints on the permitted turning power of the machine tool:

$$P_E=F_Z\cdot v\underset{\sim}{\leq}\left[\overline{P_E}\right] \tag{26}$$

where P_E - turning power.

$\left[\overline{P_E}\right]$ - the permitted turning power of the machine tool with ambiguity.

2) Constraints on the strength of the machine tool feed mechanism:

$$F_x\underset{\sim}{\leq}\left[\overline{F_m}\right] \tag{27}$$

$\left[\overline{F_m}\right]$ - the upper bound of the permissible tool walking resistance of the strength of the machine tool feed mechanism with ambiguity.

3) Bound on the surface roughness of the workpiece machining:

$$R_x\underset{\sim}{\leq}\left[\overline{R_x}\right] \tag{28}$$

where R_x - the roughness of the turned surface.

$\left[\overline{R_x}\right]$ - the upper bound of the specified value of roughness of the surface of the workpiece with ambiguity.

4) Workpiece machining accuracy constraints. In cutting shaft parts, in the cutting force F_x and F_y of the combined force, the workpiece to produce bending, so that the machining accuracy is reduced. Therefore, the establishment of machining accuracy constraints for:

$$\delta = \frac{F_{xy} \cdot l_0}{K \cdot E \cdot I} \lessapprox [\overline{\underset{\sim}{\delta}}] \tag{29}$$

where δ - the maximum bending of the workpiece during turning.

$F_{x,y}$ -- cutting force F_x, F_y of the combined force.

$$F_{x,y} = \sqrt{F_x^2 + F_y^2} \tag{30}$$

I -- the moment of inertia of the workpiece, $I = 0.05 d_w^4$.

d_w -- is the diameter of the workpiece after turning.

E --Modulus of elasticity of the workpiece material.

l_0 --The length of the workpiece between two supports.

K --Coefficient of workpiece clamping method.

$\left[\overline{\underset{\sim}{\delta}}\right]$ --The upper limit of permissible bending of the workpiece with ambiguity.

5) Constraints on the strength of the bar. When the toolbar is calculated by plane bending (ignoring the effect of F_x, F_y), the constraints on the strength of the toolbar can be established as:

$$\sigma_b = \frac{6F_a \cdot l}{BH^2} \lessapprox \left[\overline{\sigma_b}\right] \tag{31}$$

where l - the length of the cutterbar projection.

B --The width of the cross-section of the cutterbar.

H - height of the cross-section of the cutterbar.

$\left[\overline{\sigma_b}\right]$ - the upper limit of permissible bending stress of the toolbar with ambiguity.

6) Constraints on tool durability. For each type of machining and machining process system, in order to make the appropriate number of tool adjustments, tool life is given an approximate range based on experience, that is:

$$\underset{\sim}{\underline{T}} \lessapprox T \lessapprox \underset{\sim}{\overline{T}} \tag{32}$$

7) The machine tool, the tool and the workpiece have roughly one limit on the value of the cutting speed, the feed and the depth of cut, viz:

$$\underset{\sim}{\underline{v}} \lessapprox v \lessapprox \underset{\sim}{\overline{v}} \tag{33}$$

$$\underset{\sim}{\underline{f}} \lessapprox f \lessapprox \underset{\sim}{\overline{f}} \tag{34}$$

$$\underset{\sim}{\underline{a}}_p \lessapprox a_p \lessapprox \underset{\sim}{\overline{a}}_p \tag{35}$$

In each of the above constraints, the symbol "~" indicates that the operation or the quantity is ambiguous.

3.2.4. Affiliation functions for fuzzy constraints. The affiliation function of each fuzzy constraint can be determined based on the nature of the constraint. In view of the nature and characteristics of each fuzzy constraint discussed in this paragraph, a linear affiliation function is used for all constraints.

3.3. Solution flow based on MOPSO algorithm

MOPSO is a multi-objective optimization algorithm based on the group intelligence approach. The inspiration of group intelligence is inspired by the collective behavior of organisms, such as bacterial reproduction, ant colonies, bird flocks, etc. The MOPSO algorithm, as an extension and development of the single-objective particle swarm algorithm, is different from it in two ways: (1) for the process of updating the individual extreme values, it adopts the principle of "no updating if it is not dominated", i.e., individual extreme values will be updated only when a new particle dominating the current one appears. That is to say, only when a new particle that dominates the current particle appears will the individual extreme value be updated, otherwise it will not be updated; (2) for the selection of global extreme value, the particle density of the Archive set is calculated by the adaptive grid method [21].

The external archive (m -dimensional) is divided into a grid, and the mode d_i of the grid is computed in the boundary $\left(\min F_i, \max F_i\right)$ of the target space as follows:

$$d_i = \frac{\max F_i - \min F_i}{n_{grid}} \tag{36}$$

where, i represents the current iteration number; n_{grid} represents the number of grids in one dimension.

Iterating over the particles in the Archive set, recording the number/index of the grid in which they are located, and then comparing the number of particles occupying each grid, the particle density can be obtained as follows:

$$Q = \prod_{i=1}^{m} \frac{d_i}{n_i} \tag{37}$$

where n_i represents the number of particles in the grid at the i nd iteration.

Calculate the particle density size, if the result of the lower density value, that is, the greater the dispersion of particles in the grid, then randomly select a particle in the grid as the global optimal particle, which will be used as the global optimal extreme G_{best}. By selecting the small density value of the grid of the G_{best}, you can guide the next round of iteration of the update, so as to avoid falling into the local optimum.

The particle's velocity V_i, position P_i update formula is as follows:

$$\begin{aligned} v_i = {} & \omega_i \times v_i + c_1 \times rand() \times \left(P_{best} - P_i\right) \\ & + c_2 \times rand() \times \left(G_{best} - P_i\right) \end{aligned} \tag{38}$$

$$P_i = P_i + v_i \tag{39}$$

$$\omega_i = \omega_{\max} - \frac{\omega_{\max} - \omega_{\min}}{k} \times i \tag{40}$$

where, ω_i is the linearly adjusted inertia weight factor; c_1 is the individual acceleration factor; c_2 is the global acceleration factor; P_{best} represents the individual optimal extreme value; k is the maximum number of iterations; $\omega_{\max}$ is the maximum (initial) inertia weight; $\omega_{\min}$ is the minimum (termination) inertia weight; $rand\left(\ \right)$ is the random number between $\left(0,1\right)$.

The right side of equation (38) can be divided into three parts: the first part represents the inertia vector of the particle velocity (continuation of the motion trajectory of the previous particle); the second part represents the motion component of the particle converging to the individual optimal position; the third part represents the motion component of the particle converging to the global optimal position.

The flowchart of the optimization solution of MOPSO is shown in Fig. 9:

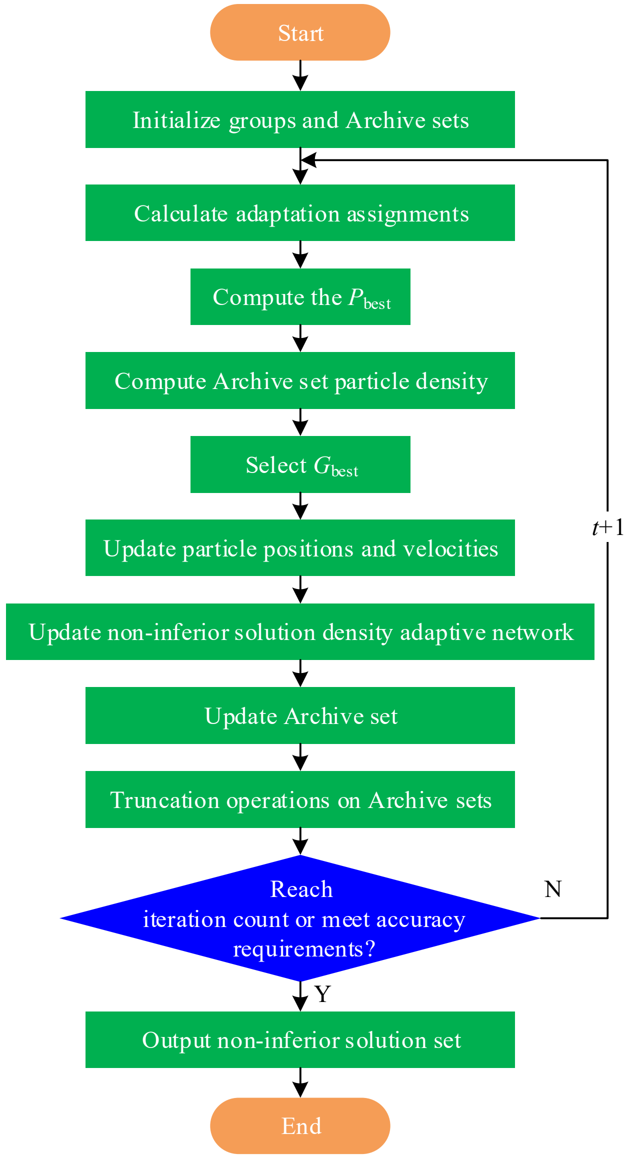

Fig. 9. Flow chart of the MOPSO algorithm

From above, the main steps of MOPSO algorithm are (1) Initialize the population and Archive set. Assign initial values to each parameter in the model, initialize the population, input the non-inferior solutions in the initial population to the Archive set, and calculate the fitness assignment and Pbest value. (2) Calculate the particle density information in the Archive set, select the optimal particle Pbest in the population (the lower the density value, the higher the probability that the particle is selected), update the non-inferiority solution density adaptive network, including the particle position and velocity, and search for the optimal solution in the range of the search space under the guidance of the G_{best} -particle and P_{best} -particle in the population. (3) Update Archive set. Update to get a new generation of population and save the non-inferior solutions in the new generation of population to the Archive set. (4) Archive set truncation operation. If the number of particles in the Archive set is judged to be more than the specified number, the excess individuals are deleted. Until the number of iterations is satisfied or the accuracy requirement is reached, the information of the particles in the Archive set, i.e., the set of non-inferior solutions, is output.

4. Reliability optimization analysis of turning machining process based on test data

4.1. Optimization conditions

1) CNC milling case test conditions:

(1) processing parts. CNC milling figure positioning piece workpiece of an irregular plane shown in Figure 10, the length of the plane is 87mm, the width is 80mm, the thickness is 50mm. workpiece material selection 38CrMoAl, processing quality requirements of surface roughness does not exceed $6.3\mu m$, processing mode for end milling. Plane milling allowance of 10mm, this example selected one of the work step optimization, in order to verify the effectiveness of multi-objective optimization method of CNC milling machining process parameters based on experimental data.

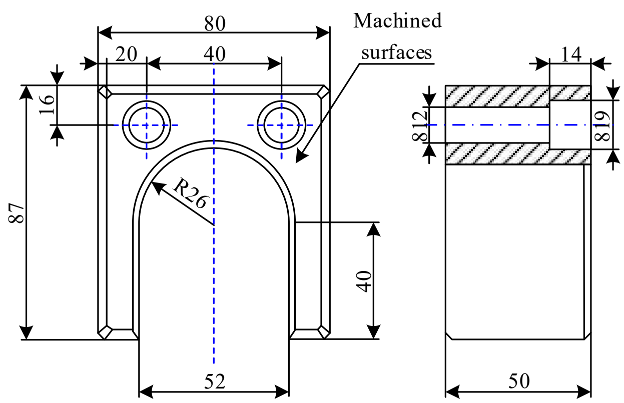

Fig. 10. The work piece for milling case

(2) CNC machine tool equipment parameters. Beijing Jingdiao SmartCNC500 model CNC machine tools are used, and its specific specifications and parameters are shown in Table 12:

Table 12. CNC Machine tool model and its parameters

Machine tool model	Maximum power of machine tool (KW)	Range of spindle speeds (rpm)	Feed speed range (mm/min)	Machine tool power coefficient η	Standby power (W)
Beijing carving smartcnc500	2.4	200-28500	1-6100	0.9	431

(3) Tool type and parameters. The tool is a high-speed steel end mill, the specific tool type and parameters are shown in Table 13:

Table 13. CNC Machine tool model and its parameters

Cutter material	Cut blade length	Cut the blade number	Knife diameter	Helical angle	Anterior angle	Back angle
High speed steel	18mm	Six	10mm	35°	16°	12°

From the cutting tool manual, the relevant calculation coefficients for milling cutter tool life can be queried as shown in Table 14:

Table 14. Relevant coefficients of calculation of milling cutter

C_T	m	r	k	EE tool-material	M tool	EP tool	EW tool
$4.52e^9$	2.07	1.15	0.91	210	0.191	1.6	4.25

The parameters related to cutting force calculation are shown in Table 15.

Table 15. Relevant coefficients of calculation of cutting force and roughness

C_F	x F	y F	y F	q F	w F	K_F
187	2	0.71	0.76	0.65	0.97	2

2) CNC turning case test conditions:

(1) Processing parts. CNC turning of a bearing housing workpiece as shown in Figure 11, for example, where the bore diameter of 52mm, turning length of 17mm, cutting allowance of 6mm. workpiece material selection of 45 steel, machining quality requirements of the surface roughness does not exceed $12.5\mu m$, the machining method selected for the bore machining. In this case, a step in the machining is selected to carry out optimization calculations to verify the effectiveness of multi-objective optimization method of CNC turning machining process parameters based on experimental data.

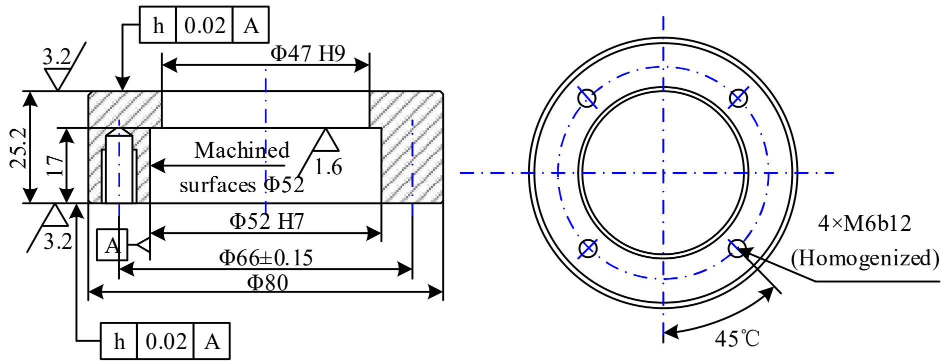

Fig. 11. The work piece for turning case

(2) CNC machine tool equipment parameters. Model C2-6136HK CNC lathe is used, and its specific specification parameters are shown in Table 16:

Table 16. CNC Machine tool model and its parameters

Machine tool model	Maximum power of machine tool (KW)	Range of spindle speeds (rpm)	Feed speed range (mm/min)	Machine tool power coefficient η	Standby power (W)
C2-6136HK	5.7	190-3200	0.04-660	0.9	355

(3) Tool type and parameters. The tool is a CNC turning tool with insert type CAMG1508-RM, the specific tool type and life parameters are shown in Table 17:

Table 17. Tool type and tool life parameters

Cutter material	Tool orthogonal rake	Tool clearance	Knife main corner cow	Knife arc radius	Blade blade number
High speed steel	19°	4°	96°	0.9mm	5

The tool embedded energy and life factors are shown in Table 18.

Table 18. Parameters of tool life and embodied energy of tool

C_T	m	r	k	EE $_{tool-material}$	M $_{tool}$	EP $_{tool}$	EW $_{tool}$
$4.21e^9$	5.90	1.35	0.44	410	0.0096	1.6	4.22

The cutting force related parameters are shown in Table 19.

Table 19. Relevant coefficients of calculation of cutting force and roughness

C_F	x F	y F	n F	K_F
336	2	0.67	0.95	1.91

4.2. *Orthogonal test implementation and roughness Ra value measurement for turning machining*

Pick factors and select levels according to orthogonal experimental design. Three factors affecting surface roughness were selected, cutting speed vc, feed f, and depth of cut ap. Three levels were taken for each factor, and a table of factor levels was listed as shown in Table 20.

Table 20. Factor levels table

	ap(mm)	F(mm/r)	vc(m/min)
1	0.2	0.11	103
2	0.4	0.19	155
3	0.6	0.28	212

Open the statistical software SPSS → switch to the variable view and name each variable as shown in Table 21.

Table 21. Variable set the table of 45 steel

Name	Type	Width	Decimals
Ap	Numerical value(N)	9	1
F	Numerical value(N)	9	3
Vc	Numerical value(N)	9	0
Ra	Numerical value(N)	9	4

Subsequently, click on the Data Acquisition option and enter the measurement length to start data acquisition. The output waveform is shown in Figure 12.

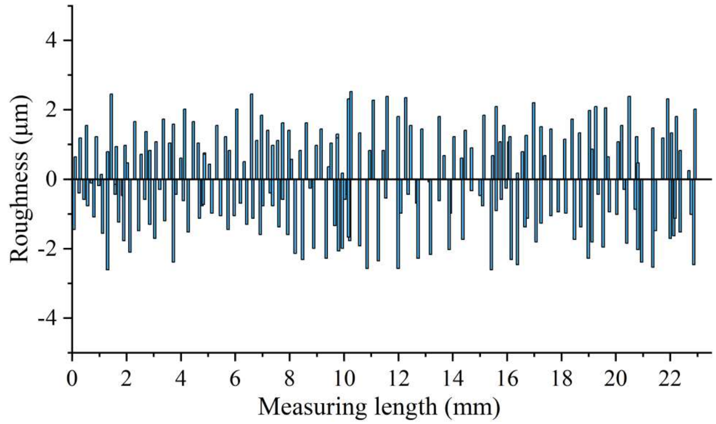

Fig. 12. Roughness kymograph

Repeat the measurements to obtain the surface roughness results measured according to the orthogonal experimental design as shown in Table 22 and enter the results into the orthogonal data table as shown in Table 23

Table 22. Surface roughness measurements

Serial number	ap (mm)	f (mm/r)	vc (m/min)	Measured value Ra (μm)				Arithmetic mean
1	0.6	0.101	210	1.748	1.63	1.6	1.724	1.618
2	0.6	0.181	160	2.961	2.487	2.564	2.909	2.673
3	0.6	0.261	110	4.03	3.99	4.009	4.147	3.987
4	0.4	0.261	210	4.597	3.413	3.54	3.612	3.733
5	0.4	0.101	160	1.689	1.25	1.352	1.368	1.358
6	0.4	0.181	110	2.814	2.679	2.722	2.28	2.567
7	0.2	0.181	210	2.453	2.402	2.335	2.352	2.328
8	0.2	0.261	160	3.629	3.814	3.808	3.439	3.615
9	0.2	0.101	110	1.604	1.324	1.274	1.289	1.316

Table 23. The orthogonal experiment data tables

ap(mm)	f(mm/r)	vc(m/min)	Ra(μm)
4(0.6)	2(0.09)	4(2100	1.847
4	3(0.17)	3(160)	2.902
4	4(0.27)	2(110)	4.216
3(0.4)	4	4	3.962
3	2	3	1.477
3	3	2	2.557
2(0.2)	3	4	3.844
2	4	3	1.545
2	2	2	1.855

The system automatically generates univariate ANOVA results for 45 steel orthogonal test turning processing as shown in Table 24. The mean value of variance in the table is the average of the same level of test indicators for each factor. That is, the mean value of variance = 2.549 when ap is taken as 0.2. Other data are calculated in the same way. As can be seen from the table, when the distribution of measurement data is more dispersed (i.e., the data fluctuate more near the mean of variance), the sum of the squares of the differences between the individual data and the mean is larger, i.e., the variance is larger; when the distribution of measurement data is more concentrated (i.e., the data fluctuate less near the mean of variance), the sum of the squares of the differences between the individual data and the mean of variance is smaller, i.e., the variance is smaller.

Table 24. Univariate analysis of variance table three factors

ap	Variance mean	f	Variance mean	vc	Variance mean
0.2	2.549	0.101	1.709	110	2.623
0.4	2.682	0.181	2.801	160	2.549
0.5	2.888	0.261	4.056	210	2.561

4.3. Optimization results and analysis

1) Optimization of algorithm parameters and performance effect. The basic parameters are as follows: learning factor c_1 and c_2 are taken as 1; inertia weights $\omega_{\max}$ and $\omega_{\min}$ are taken as 0.2 and 0.6; the number of populations is 80; the number of iterations is 100; and the speeds $V_{\max}$ and $V_{\min}$ are 1.5 and -1.5, respectively. Matlab programming is used to solve the model, and Fig. 13 is a comparison of convergence front of the algorithms at the 70th generation of the run, and the blue solid line is the convergence front of the improved algorithm, and the green solid line is the convergence front of the standard particle swarm algorithm, which is closer to the real one. The green solid line is the convergence frontier of the standard particle swarm algorithm. From the figure, it can be seen that the convergence speed of the algorithm using MOPSO is faster and the convergence frontier is closer to the real Pareto frontier.

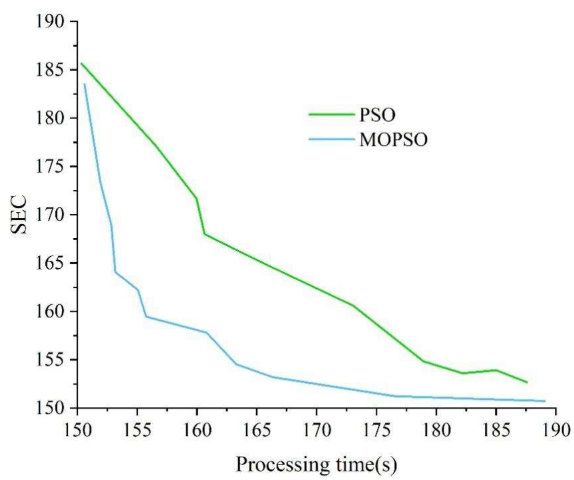

Fig. 13. The convergence of algorithm

2) Optimization results analysis. Multi-objective particle swarm algorithm and single-objective particle swarm algorithm are used to solve the optimization model respectively, and there are six types of optimization schemes: $SEC^{dir+indir}\&T_p$

SchemeI: Multi-objective optimization text with SEC^{dir} and processing time as optimization objectives.

SchemeII: Multi-objective optimization text with $SEC^{dir+indir}$ and processing time as the optimization objective.

SchemeIII: A single-objective optimization text with SEC^{dir} as the optimization objective.

SchemeIV: A single-objective optimization scheme with $SEC^{dir+indir}$ as the optimization objective.

SchemeV: Single-objective optimization with machining time as the optimization objective.

SchemeVI: Experienced process parameters given by skilled operators on the spot.

(1) Optimization results of milling process parameters. The process parameters of the six optimization schemes are brought into the formula, and the results of the optimization comparison of the six parameters are summarized as shown in Table 25.

Comparison of milling optimization scheme II and scheme IV shows that when $SEC^{dir+indir}$ and machining time are the optimization objectives, although the value of $SEC^{dir+indir}$ is 5.9% higher than the optimization of $SEC^{dir+indir}$ alone, the value of time is reduced by 11.1%; comparison of scheme II and scheme V shows that although the value of time is 2.4% higher than the optimization of machining time of CNC milling process parameter scheme alone, the value of $SEC^{dir+indir}$ is reduced by 31.9%. Comparison of scenarios I and II shows that the specific energy considering indirect energy consumption is affected by the internal energy of the tool, and the process parameters are smaller than those of the optimized scenario I. However, comparing the values of the specific energy of the two scenarios, it can be seen that, although the value of SEC^{dir} of scenario II is 8.9% higher than that of scenario I, the value of $SEC^{dir+indir}$ is reduced by 18.6%. It can be seen that the multi-objective optimization of energy efficiency considering indirect energy consumption can greatly reduce the generation of indirect energy consumption in the machining process, so that the energy efficiency of the CNC machining system can achieve a more energy-saving and emission reduction effect.

Table 25. The optimization results for milling parameters

Type	n(r/min)	f_z(mm/t)	a_p(mm)	a_e(mm)	T_p(s)	SEC ^{dir}	SEC $^{dir+indir}$
SchemeI	3727	0.0283	0.398	3.994	165.37	152.54	6566.45
SchemeII	2909	0.0276	0.388	3.993	156.64	166.13	5592.23
SchemeIII	4433	0.0278	0.507	4.009	180.9	151.55	7076.76
SchemeIV	2455	0.0271	0.507	4.009	173.99	170.74	5278.8
SchemeV	3398	0.0274	0.307	3.928	153.08	177.26	7365.4
SchemeVI	2739	0.0315	0.262	3.025	191.63	189.21	10028.9

(2) Turning machining process parameters optimization results. The process parameters of the six optimization schemes are brought into the formula, and the summary of the six process parameters optimization comparison results are shown in Table 26.

Comparison of the optimized combinations of turning and milling operations under each objective shows that the results for turning and milling are basically the same. Comparing turning machining scenarios I and III, it can be seen that when optimizing the process parameter scenarios with SEC^{dir} and machining time at the same time, although the value of SEC^{dir} is 10.9% higher than the optimization of SEC^{dir} alone, the value of time decreases by 13.8%; similarly, comparing scenarios I and V, the value of machining time of scenario I is 7.8% higher but the value of SEC^{dir} decreases by 22.2%. Comparing the turning machining scenarios II and IV, it can be seen that when both $SEC^{dir+indir}$ and machining time are used as the optimization objectives, although the value of $SEC^{dir+indir}$ is 9.32% higher than the optimization of $SEC^{dir+indir}$ alone, the value of time decreases by 13.1%; and when comparing scenario II with scenario V, which optimizes the machining time alone, the value of $SEC^{dir+indir}$ decreases by 29.8%, although the value of time increases by 3.7%.

Table 26. The optimization results

Type	v_c(r/min)	f(mm/t)	a_p(mm)	T_p(s)	SEC^{dir}	$SEC^{dir+indir}$
SchemeI	81.99	0.277	1.219	96.73	12.77	27.63
SchemeII	58.02	0.265	1.2	93.16	13.53	22.16
SchemeIII	89.98	0.278	1.302	112.16	11.52	30.93
SchemeIV	52.61	0.267	1.312	107.24	14.68	20.27
SchemeV	79.88	0.276	0.809	89.72	16.42	31.55
SchemeVI	48.32	0.23	0.757	119.28	19.41	37.15

From the optimization results of turning and milling machining, it can be seen that the method proposed in this paper can balance the two objectives, so that the optimization results can be coordinated between the time and energy efficiency objectives, and the selection of the multi-objective energy efficiency optimization scheme is more superior than the single pursuit of the highest energy efficiency or the lowest time in the cutting process. In addition, in terms of the energy loss of the entire CNC machining system, the energy efficiency multi-objective optimization process that considers indirect energy consumption improves the energy saving and emission reduction effect than the optimization result of the energy efficiency multi-objective scheme that only considers direct energy consumption because it takes into account both direct and indirect energy consumption in the machining process.

The trends of total machining energy consumption (blue line), cutting energy consumption (green line), tool change energy consumption (red line) and no-load energy consumption (orange line), and tool contained energy (yellow line) with the increase of material removal rate are shown in Fig. 14. When the material removal rate is small, the no-load energy consumption decreases with the increase of the material removal rate, but with the increase of the MRR, the trend gradually becomes weaker until it becomes constant, so the total machining energy consumption is mainly affected by the cutting energy consumption, the tool change energy consumption and the tool internal energy.

In the region from point C to point D, the cutting energy consumption decreases significantly with the increase of MRR due to the sharp reduction of cutting time. The total energy consumption is mainly dominated by the cutting energy consumption with a decreasing trend, although the tool change energy consumption and the tool internal energy have a certain increasing trend. Beyond point D, the decreasing trend of cutting energy consumption becomes flat as MRR continues to rise. In this region, although the increase in MRR reduces the cutting time but due to the increase in cutting area leads to larger deformation force and friction force, the cutting force also increases, so the cutting energy consumption decreases in general while at the same time is not as drastic as before.

In the region from D to E, due to the higher MRR, the tool wear increases and the tool change time increases, resulting in an exponential function increase in the tool change energy consumption, in addition to the sharp increase in the tool embedded energy consumption causing a significant rise in the total energy consumption. Although the total energy consumption increases with MRR during this time, SEC^{dir} (black line) and $SEC^{dir+indir}$ (purple line) still show a decreasing trend. When MRR increases to point E, $SEC^{dir+indir}$ decreases to the lowest point, after which $SEC^{dir+indir}$ has a clear upward trend influenced by the tool internal energy.

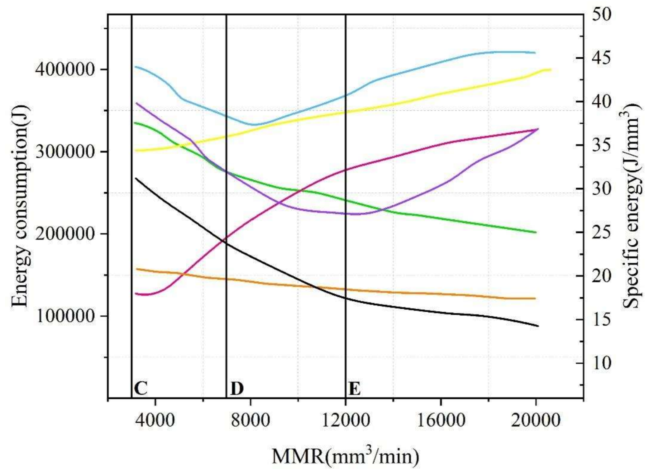

Fig. 14. SEC as a function of MRR for turning case

5. Conclusion

In this paper, the Gumbel Copula function model is identified as the optimal model by the AIC criterion, and it is introduced into Monte Carlo simulation, and the chatter time-varying reliability model of the turning machining system is established for the turning machining process in aerospace manufacturing.

The specific work and conclusions are summarized as follows:

1) VC-MSS method and Monte Carlo method with Copula function were used to analyze the reliability of the turning system, and it was found that the simulated points obtained by sampling had almost the same correlation degree with the original sample points, and the probability density characteristics of each simulated variable were almost the same with the original sample data. The accuracy of the Gumbel-Copula function model to the original sample and the simulation points are verified.

2) When the turning width is b-0.63mm, the stability of the turning flutter is the best, the instability is the least, and the turning processing system operates well at the full speed.

3) The mathematical model of fuzzy optimization of turning process aiming at the lowest machining cost is solved by multi-objective particle swarm optimization algorithm. The results show that the method proposed in this paper can balance the two objectives, so that the optimization results can be coordinated between the time and energy efficiency objectives. The multi-objective energy efficiency optimization scheme is more advantageous than the single pursuit of the highest energy efficiency or the lowest time in the cutting process.

Acknowledgments

We would like to express our appreciation to Provincial Doctoral Research Start-up Fund Project of Science and Technology Department of Liaoning Province (2023BS147) and the Fundamental Research Funds for the Universities of Liaoning Province(LJ212410143081) and Open Fund of Key Laboratory of Fundamental Science for National Defense of Aeronautical Digital Manufacturing Process of Shenyang Aerospace University (SHSYS202402) for supporting this research.

References

[1] Çelik, H. S. (2020). Root Cause Analysis Methods for The Design of Aviation Parts. Journal of Aviation, 4(2), 1-9.

[2] Grzesik, N., & Iwan, T. (2017). The Application of Probability Elements in Optimizing Supply of Spare Parts and Components in Aviation. Journal of KONBiN, 44(1), 359.

[3] Zhao, B., Wang, Y., Peng, J., Wang, X., Ding, W., Lei, X., ... & Das, R. (2024). Overcoming challenges: advancements in cutting techniques for high strength-toughness alloys in aero-engines. International Journal of Extreme Manufacturing, 6(6), 062012.

[4] Yurtkuran, H. (2021). An evaluation on machinability characteristics of titanium and nickel based superalloys used in aerospace industry. İmalat Teknolojileri ve Uygulamaları, 2(2), 10-29.

[5] Ţîţu, A. M., Sandu, A. V., Pop, A. B., Ţîţu, Ş., Frăţilă, D. N., Ceocea, C., & Boroiu, A. (2020). Design of experiment in the milling process of aluminum alloys in the aerospace industry. Applied Sciences, 10(19), 6951.

[6] You, S. H., Lee, J. H., & Oh, S. H. (2019). A study on cutting characteristics in turning operations of titanium alloy used in automobile. International Journal of Precision Engineering and Manufacturing, 20, 209-216.

[7] Kim, J., & Kang, B. (2018). Machining characteristics of micro lens mold in laser-assisted micro-turning. Journal of Mechanical Science and Technology, 32, 1769-1774.

[8] Tajne, A., Gupta, T. V. K., Ramani, H., & Joshi, Y. (2024). A critical review on the machinability aspects of nickel and cobalt based superalloys in turning operation used for aerospace applications. Advances in Materials and Processing Technologies, 10(2), 833-866.

[9] Liu, J., Chen, G., Zhao, L., Yu, Z., & Jia, X. (2023). Research status and development trend of cutting surface integrity of aerospace alloy materials. The International Journal of Advanced Manufacturing Technology, 127(1), 45-63.

[10] Sangwan, K. S., & Sihag, N. (2019). Multi-objective optimization for energy efficient machining with high productivity and quality for a turning process. Procedia CIRP, 80, 67-72.

[11] Abolghasema, S., & Cubides, N. M. (2022). Optimization of machining parameters for product quality and productivity in turning process of aluminum. Ingeniería y universidad, 26, 1.

[12] Negrău, D. C., Grebenisan, G., Gherghea, I. C., & Anton, D. (2021). The advantages of combining 3D printing with turning process. Case study. In MATEC Web of Conferences (Vol. 343, p. 02010). EDP Sciences.

[13] Urbikain, G., Alvarez, A., López de Lacalle, L. N., Arsuaga, M., Alonso, M. A., & Veiga, F. (2017). A reliable turning process by the early use of a deep simulation model at several manufacturing stages. Machines, 5(2), 15.

[14] Patil, R. B., Kothavale, B. S., Waghmode, L. Y., & Joshi, S. G. (2017). Reliability analysis of CNC turning center based on the assessment of trends in maintenance data: a case study. International Journal of Quality & Reliability Management, 34(9), 1616-1638.

[15] Rao, T. B. (2022). Reliability analysis of the cutting tool in plasma-assisted turning and prediction of machining characteristics. Australian Journal of Mechanical Engineering, 20(4), 1020-1034.

[16] En, X., Zhang, Y., Huang, X., Li, Y., & Yang, G. (2022). Time-varying reliability and global sensitivity analysis of regenerative chatter stability in turning considering tool wear. Mechanics Based Design of Structures and Machines, 50(12), 4084-4104.

[17] Syropoulos, A., & Grammenos, T. (2020). A modern introduction to fuzzy mathematics. John Wiley & Sons.

[18] Khaoula El Asame,Halima Zaari,Abdessamia Rhazaoui,Abdelilah Benyoussef & Abd Allah El Kenz. (2024). Magnetic properties and magnetocaloric effect of Gd3In compound: DFT and Monte Carlo simulations. Chemical Physics Letters141201-.

[19] Wahyu Triyoso. (2024). Applying the Akaike Information Criterion (AIC) in earthquake spatial forecasting: a case study on probabilistic seismic hazard function (PSHF) estimation in the Sumatra subduction zone. Geomatics, Natural Hazards and Risk(1),

[20] Gao Zhaokui & Xu Guoqiang. (2024). Evaluation of green pastoral residence in Grassland of Inner Mongolia based on fuzzy mathematics. E3S Web of Conferences

[21] Yansong Zhang,Yanmin Liu,Xiaoyan Zhang,Qian Song,Aijia Ouyang & Jie Yang. (2025) .Multi-objective Particle Swarm Optimization with Integrated Fireworks Algorithm and Size Double Archiving. International Journal of Computational Intelligence Systems(1),2-2.